ELSEVIER

Biophysical Chemistry 95 (2002) 59–68

Biophysical Chemistry

www.elsevier.com/locate/bpc

A new approximate whole boundary solution of the Lamm differential equation for the analysis of sedimentation velocity experiments

Joachim Behlke*, Otto Ristau

Max Delbrück Center for Molecular Medicine, D-13092 Berlin, Germany

Received 10 September 2001; received in revised form 20 November 2001; accepted 26 November 2001

Abstract

Sedimentation velocity is one of the best-suited physical methods for determining the size and shape of macromolecular substances or their complexes in the range from 1 to several thousand kDa. The moving boundary in sedimentation velocity runs can be described by the Lamm differential equation. Fitting of suitable model functions or solutions of the Lamm equation to the moving boundary is used to obtain directly sedimentation and diffusion coefficients, thus allowing quick determination of size, shape and other parameters of macromolecules. Here we present a new approximate *whole boundary* solution of the Lamm equation that simultaneously allows the specification of sedimentation and diffusion coefficients with deviations smaller than 1% from the expected values.

Keywords: Analytical ultracentrifugation; Sedimentation coefficient; Diffusion coefficient; Molecular mass; Proteins

1. Introduction

Analytical ultracentrifugation is a valuable tool to characterize the solution structure of macromolecules especially their molecular masses, gross conformation and interaction [1,2]. Alternative to the more time-consuming sedimentation equilibrium experiments, which yield the molecular mass data, directly, sedimentation velocity runs can provide the corresponding values from the moving boundary in a few hours. This can be of advantage for substances which are sensitive to denaturation.

Mass transport in a sector-shaped cell rotating in an analytical ultracentrifuge can be described by the Lamm equation [3], a partial differential equation. But closed analytical solutions of the transport equation for the ultracentrifuge are not available.

Approximately four decades ago Fujita [4] developed approximate solutions of the Lamm equation describing radial concentration profiles of sedimentation velocity experiments.

For a long time the fitting procedure of such concentration profiles with solution functions con-

* Corresponding author. Max Delbrück Center for Molecular Medicine, Robert Rössle Str. 10, D-13125 Berlin, Germany. Tel.: +49-30-9406-2802; fax: +49-30-9406-2802.

E-mail address: behlke@mdc-berlin.de (J. Behlke).

0301-4622/02/$ - see front matter
PII: S0301-4622(01)00248-4

taining several error functions seemed computationally too difficult for subsequent applications. Later on some efforts were made to get reliable results by other approximate solutions of the Lamm equation [5–8]. Furthermore, numerical solutions of the Lamm equation [9–15] have been reported. Nevertheless, one of Fujita's approximate solutions (Eq. 2.280 in Fujita [4]) of the Lamm equation describing the whole boundary is particularly well suited for the direct determination of sedimentation and diffusion coefficients of small proteins with a molecular mass of 10–20 kDa or lower by fitting the radial concentration distributions [8]. Here we demonstrate a new model function that allows determination of the sedimentation and diffusion coefficients of *monodisperse* proteins with deviations smaller than 1% from the expected values.

2. Theory

2.1. General remarks

The isothermal sedimentation in a two-component system (one sedimentating species) where the partial specific volumes, the sedimentation coefficient s and the diffusion coefficient D are constant is described by the following partial differential equation of second order first derived by Lamm [3]:

$$\frac{\partial c}{\partial t} = \frac{1}{r}\frac{\partial}{\partial r}\left[rD\frac{\partial c}{\partial r} - s\omega^2 r^2 c\right] \tag{1}$$

with c = concentration, r = radial distance measured from the axis of rotor, t = running time, ω = angular rotor speed.

In order to facilitate the analysis of the Lamm equation the following dimensionless variables are generally introduced [4]:

$$\left(\frac{r}{r_m}\right)^2 = x, \quad 2s\omega^2 t = \tau, \quad \frac{2D}{s\omega^2 r_m^2} = \varepsilon, \quad \frac{c}{c_0}e^{\tau} = \theta \tag{2}$$

c_0 = loading concentration, r_m = meniscus position.

In terms of these quantities Eq. (1) may be written

$$\frac{\partial \theta}{\partial \tau} = \varepsilon x\frac{\partial^2 \theta}{\partial x^2} + (\varepsilon - x)\frac{\partial \theta}{\partial x} \tag{3}$$

In 1962 Fujita [4] published an approximate solution of the Lamm Eq. (3) of the Archibald type. This solution was improved in 1998 by Behlke and Ristau [16] and implemented into our program Lamm. The simplified Lamm equation used was

$$\frac{\partial \theta}{\partial \tau} = a\varepsilon\frac{\partial^2 \theta}{\partial x^2} + (\varepsilon - a)\frac{\partial \theta}{\partial x} \tag{4}$$

The constant value a was $a = 1$ for the meniscus solution and

$$a = \left(\frac{r_b}{r_m}\right)^2$$

for the bottom part. As communicated in Behlke and Ristau [16] this approximate solution consists of two additive parts. The first three terms are a solution of the simplified Lamm equation considering the meniscus boundary condition only and the last three terms are a solution considering the bottom boundary only. When the two partial solutions are independent from each other the sum of both parts is a correct whole boundary solution. The two parts are independent solutions when the bottom part does not influence the boundary condition for the meniscus part and the meniscus part does not influence the boundary condition for the bottom part. These conditions are fulfilled: (a) when the concentration and the gradient dc/dr of the bottom part are zero at the meniscus radius; and (b) the gradient of the meniscus part is zero, and the reduced concentration c/c_0 has the value $\exp(-\tau)$ (the reduced plateau concentration) at the bottom radius. Some deviation is tolerable as ascertained by extensive tests on synthetic data sets. Both conditions (a, b) are fulfilled numerically acceptable when the reduced gradient $(dc/dr)/c_0$ of the bottom trace and the reduced gradient of the meniscus trace have the same slope $< 2.5(1+35\varepsilon)$ at a common radius point near the bottom which is the nearest possible one. The gradient of the bottom trace at the meniscus is then always < 0.005 and the amplitude < 0.0005. The gradient of the meniscus trace at the bottom is < 0.5 but always smaller than 1% of the slope

of the bottom trace which is responsible for the calculation of the bottom boundary condition [Eq. (10)] and the amplitude always >0.95. To measure the degree to which deviation can be tolerated, a control parameter is included in our program LAMM.

The approximate solution [16] in an alternative form is

$$\theta=\frac{1}{2}\left\{erfc\left(\frac{\tau(f-\varepsilon)-x+1}{2\sqrt{f\ \varepsilon\ \tau}}\right)-\frac{f}{\varepsilon}\exp\left(\frac{(x-1)(f-\varepsilon)}{f\ \varepsilon}\right)erfc\left(\frac{\tau(f-\varepsilon)+x-1}{2\sqrt{f\ \varepsilon\ \tau}}\right)+\frac{f+\varepsilon}{\varepsilon}\exp\left(\frac{\varepsilon+x-1}{\varepsilon}\right)erfc\left(\frac{\tau\,(f+\varepsilon)+x-1}{2\sqrt{f\ \varepsilon\ \tau}}\right)-erfc\left(\frac{z-\tau(\varepsilon_b-1)}{2\sqrt{\varepsilon_b\tau}}\right)-\frac{1}{\varepsilon_b}\exp\left(\frac{(\varepsilon_b-1)z}{\varepsilon_b}\right)erfc\left(\frac{z+\tau(\varepsilon_b-1)}{2\sqrt{\varepsilon_b\tau}}\right)+\frac{1+\varepsilon_b}{\varepsilon_b}\exp\left(\frac{\tau\varepsilon_b-z}{\varepsilon_b}\right)erfc\left(\frac{z-\tau(\varepsilon_b+1)}{2\sqrt{\varepsilon_b\tau}}\right)\right\} \tag{5}$$

with

$$x_b=\frac{r_b^2}{r_m^2},\quad f=1+0.5(\mathrm{e}^{\tau}-1) \tag{6}$$

r_m or r_b = radius positions at meniscus and cell base. The parameter f is a supplementary introduced empirical quantity that improves the accuracy of estimated parameters. The error function (*erf*) and the complementary error function (*erfc*) are defined by

$$erfc(x)=1-erf(x)=1-\frac{2}{\sqrt{\pi}}\int_0^x \mathrm{e}^{-z^2}\mathrm{d}z$$

A new distinctly improved whole boundary model function can be developed based on two independent solutions of slightly different differential equations for the meniscus and bottom part by using new better approximated Lamm equations that are more complicated than Eq. (4) but which nevertheless can be analytically integrated.

2.2. The improved approximate solution for the meniscus part

Such better approximation to the exact Lamm Eq. (3) is the following differential equation.

$$\frac{\partial\theta}{\partial\tau}=\varepsilon x\,\frac{\partial^2\theta}{\partial x^2}+\left(\varepsilon\frac{1+\sqrt{x}}{2}-\sqrt{x}\right)\frac{\partial\theta}{\partial x} \tag{7}$$

In contrast to Eq. (4) with $a=1$, function (7) is expected to yield also suitable results for x values slightly larger than 1. By substitution of

$$w=2\left(\sqrt{x}-1\right) \tag{8}$$

this linear differential equation can be transferred to a linear differential equation with constant coefficients.

$$\frac{\partial\theta}{\partial\tau}=\varepsilon\,\frac{\partial^2\theta}{\partial w^2}+\left(\frac{\varepsilon}{2}-1\right)\frac{\partial\theta}{\partial w} \tag{9}$$

A solution of this differential equation with reference to the initial and boundary conditions [Eq. (10)] at meniscus can be achieved using the Laplace transformation:

$$\theta=1\quad w>=0,\quad \tau=0 \tag{10}$$

$$\varepsilon\frac{\partial\theta}{\partial w}=\theta\quad w=0,\quad \tau>0$$

The solution is:

$$\frac{2\,c\,\mathrm{e}^{\tau}}{c_0}=erfc\left(\frac{b\,\tau-w}{2\sqrt{\varepsilon\,\tau}}\right)-\frac{1}{(1-b)}\exp\left(\frac{b\,w}{\varepsilon}\right)erfc\left(\frac{w+b\,\tau}{2\sqrt{\varepsilon\,\tau}}\right)+\frac{(2-b)}{(1-b)}\exp\left(\frac{w+\tau(1-b)}{\varepsilon}\right)erfc\left(\frac{w+(2-b)\,\tau}{2\sqrt{\varepsilon\,\tau}}\right) \tag{11}$$

with the following substitutions

$$b=1-\varepsilon/2,\quad w=2\left(\frac{r}{r_m}-1\right) \tag{12}$$

Each term of the solution of the simplified Lamm equation with constant coefficients is also

a solution of the same differential equation without boundary conditions. The first term of Eq. (11) addresses the moving boundary whereas the other two terms are necessary to fulfill the meniscus boundary condition. A further improvement of the solution can be obtained by substituting the first term of Eq. (11) by a corresponding term, which satisfies an even more exact approximation of the Lamm equation describing the moving boundary. One possibility for such a substitution is provided by an equation derived by Hiester and Vermeulen [17], which addresses the moving boundary, but in synthetic boundary cells. Although substitution of the first term by the mentioned function leads to a violation of the meniscus boundary condition this disadvantage is numerically insignificant, as shown by analysis of simulated curves generated according to Claverie et al. [9] and Cox and Dale [10]. Of course, when meniscus depletion is achieved only this first substituted term is important for the accuracy of the solution. The corresponding dominant term of the Hiester–Vermeulen equation is:

$$\frac{2c\mathrm{e}^{\tau}}{c_0} = erfc\left(\frac{1-\sqrt{x\mathrm{e}^{-\tau}}}{\sqrt{\varepsilon(1-\mathrm{e}^{-\tau})}}\right) = erfc\left(\frac{\mathrm{e}^{\tau/2}-\sqrt{x}}{\sqrt{\varepsilon(\mathrm{e}^{\tau}-1)}}\right) \quad (13)$$

It can be shown that this function is a solution of the differential equation

$$\frac{\partial\theta}{\partial\tau} = \varepsilon x\frac{\partial^2\theta}{\partial x^2} + \left(\frac{\varepsilon}{2}-x\right)\frac{\partial\theta}{\partial x} \quad (14)$$

with the initial conditions

$\theta = 1 \quad \tau = 0, \quad x \geq 1$

$\theta = 0 \quad \tau = 0, \quad x < 1$

For $\varepsilon \ll 1$ this equation is a good approximation of the exact Lamm equation [Eq. (3)]. Furthermore, an improvement can be made by adding an auxiliary term to the numerator.

$$\frac{2c\mathrm{e}^{\tau}}{c_0} = erfc\left(\frac{\mathrm{e}^{\tau/2}-\sqrt{x}+0.5\varepsilon(1-\mathrm{e}^{\tau/2})}{\sqrt{\varepsilon(\mathrm{e}^{\tau}-1)}}\right) = erfc\left(\frac{2b(\mathrm{e}^{\tau/2}-1)-w-2}{2\sqrt{\varepsilon(\mathrm{e}^{\tau}-1)}}\right) \quad (15)$$

This improved function satisfied the differential equation

$$\frac{\partial\theta}{\partial\tau} = \varepsilon x\frac{\partial^2\theta}{\partial x^2} + \left(\frac{\varepsilon}{2}\left(1+\sqrt{x}\right)-x\right)\frac{\partial\theta}{\partial x} \quad (16)$$

Eq. (16) is a very good approximation of the exact Lamm Eq. (3), particularly when considering small changes of the variable x, which occur generally in centrifuge experiments. However, with increasing x, the factor $\left(1+\sqrt{x}\right)/2$ in Eq. (16) exceeds the exact value of 1. Indeed, for small ε ($\varepsilon \ll x$) the error is negligible, but noticeable for large values of ε true for very small molecules. A slightly modified form of Eq. (16) rectifies this deficiency.

$$\frac{2c\mathrm{e}^{\tau}}{c_0} = erfc\left(\frac{\mathrm{e}^{\tau/2}-\sqrt{x}+0.25\ \varepsilon\ (\mathrm{e}^{-\tau/2}-\mathrm{e}^{\tau/2})}{\sqrt{\varepsilon(\mathrm{e}^{\tau}-1)}}\right) \quad (17)$$

Function (17) is a solution of the differential equation:

$$\frac{\partial\theta}{\partial\tau} = \varepsilon x\frac{\partial^2\theta}{\partial x^2} + \left(\frac{\varepsilon}{2}\left(1+\mathrm{e}^{-\tau/2}\sqrt{x}\right)-x\right)\frac{\partial\theta}{\partial x} \quad (18)$$

This formulation means that the ε term (in brackets) always has the nearly correct value at the midpoint of the boundary. This is true because displacement from the meniscus is described with great exactness by

$$\sqrt{x_*} = \mathrm{e}^{\tau/2} \quad \text{or} \quad x_* = \mathrm{e}^{\tau} \quad (19)$$

To achieve a solution it is crucial that the correct ε-value exists at the midpoint, since at this position the solution function is the steepest.

2.3. An improved solution for the bottom part

The roughly approximate Lamm Eq. (4) with $a = (r_b/r_m)^2$ used for the bottom part can also be

replaced by a more improved function. The new function strongly resembles those for the meniscus part [Eq. (7)] but is now adapted to the bottom. This function yields more reliable results for radius values near the bottom.

With the following substitution into Eq. (3)

$$x = y\frac{r_b^2}{r_m^2} \tag{20}$$

one obtains the following alternative Lamm equation.

$$\frac{\partial\,\theta}{\partial\,\tau} = \varepsilon_b\, y\,\frac{\partial^2\theta}{\partial\, y^2} + (\varepsilon_b - y)\,\frac{\partial\,\theta}{\partial\, y} \tag{21}$$

with

$$y = \frac{r^2}{r_b^2}, \quad \varepsilon_b = \frac{2D}{s\, r_b^2\omega^2} \tag{22}$$

As mentioned for Eq. (3), Eq. (21) also does not allow a direct closed analytical solution. Therefore, an analogous approximation as that used for the meniscus part is employed.

$$\frac{\partial\theta}{\partial\tau} = \varepsilon_b\, y\frac{\partial^2\theta}{\partial y^2} + \left(\frac{\varepsilon_b}{2}\left(1+\sqrt{y}\right) - \sqrt{y}\right)\frac{\partial\theta}{\partial y} \tag{23}$$

In contrast to function (4) with $a = (r_b/r_m)^2$ Eq. (23) is a good approximation of the exact Lamm equation for y values near 1 (close to the bottom), but not for y data near to the meniscus ($y<1$). Using an analog substitution as mentioned above, equation

$$z = 2\left(\sqrt{y} - 1\right) \tag{24}$$

can be again transferred into a differential equation with constant coefficients.

$$\frac{\partial\theta}{\partial\tau} = \varepsilon_b\,\frac{\partial^2\theta}{\partial z^2} + \left(\frac{\varepsilon_b}{2} - 1\right)\frac{\partial\theta}{\partial z}, \quad \varepsilon_b = \frac{2D}{r_b^2 s\omega^2} \tag{25}$$

Taking into account the initial and boundary conditions for the bottom, the solution is:

$$\frac{2c}{c_0}\mathrm{e}^{\tau} = 2 - erfc\left(\frac{d\,\tau - z}{2\sqrt{\varepsilon_b\,\tau}}\right) - \frac{1}{1-d}\exp\left(\frac{d\,z}{\varepsilon_b}\right)erfc\left(\frac{-z-d\,\tau}{2\sqrt{\varepsilon_b\tau}}\right) + \frac{2-d}{1-d}\exp\left(\frac{(1-d)\,\tau + z}{\varepsilon_b}\right)erfc\left(\frac{-z-(2-d)\,\tau}{2\sqrt{\varepsilon_b\tau}}\right) \tag{26}$$

where

$$\varepsilon_b = \frac{2D}{r_b^2\, s\,\omega^2}, \quad d = 1 - \varepsilon_b/2, \quad z = 2\left(\frac{r}{r_b} - 1\right) \tag{27}$$

2.4. The whole boundary solution

The violation of the meniscus boundary condition mentioned above can be nearly overcome by replacing the variable τ in the last two terms of Eq. (11) with the term $2^*(\mathrm{e}^{\tau/2}-1)$. This time the relation is more correct for describing the moving boundary. The complete solution is expressed by Eqs. (11), (17) and (26).

$$\begin{aligned}\frac{2c\mathrm{e}^{\tau}}{c_0} = {} & erfc\left(\frac{\mathrm{e}^{\tau/2} - 0.5w - 1 + 0.25\varepsilon(\mathrm{e}^{-\tau/2} - \mathrm{e}^{\tau/2})}{\sqrt{\varepsilon(\mathrm{e}^{\tau}-1)}}\right) \\ & - \frac{1}{(1-b)}\exp\left(\frac{b\,w}{\varepsilon}\right)erfc\left(\frac{w + 2b(\mathrm{e}^{\tau/2}-1)}{2\sqrt{2\varepsilon\,(\mathrm{e}^{\tau/2}-1)}}\right) \\ & + \frac{(2-b)}{(1-b)}\exp\left(\frac{w + 2(\mathrm{e}^{\tau/2}-1)\,(1-b)}{\varepsilon}\right) \\ & \times erfc\left(\frac{w + 2(2-b)(\mathrm{e}^{\tau/2}-1)}{2\sqrt{2\varepsilon(\mathrm{e}^{\tau/2}-1)}}\right) \\ & - erfc\left(\frac{d\,\tau - z}{2\sqrt{\varepsilon_b\,\tau}}\right) - \frac{1}{1-d}\exp\left(\frac{d\,z}{\varepsilon_b}\right) \\ & \times erfc\left(\frac{-z-d\,\tau}{2\sqrt{\varepsilon_b\tau}}\right) \\ & + \frac{2-d}{1-d}\exp\left(\frac{(1-d)\,\tau + z}{\varepsilon_b}\right) \\ & \times erfc\left(\frac{-z-(2-d)\,\tau}{2\sqrt{\varepsilon_b\tau}}\right)\end{aligned} \tag{28}$$

The first three terms build a function of Faxén type describing the moving boundary with the following plateau region. The first term [Eq. (17)] is responsible for the moving boundary and the other two for accomplishment the meniscus boundary condition taken from Eq. (11) with slightly

changed expression for the reduced time parameter (τ) mentioned above. The last three terms [Eq. (26)] describe the increase of the concentration near the bottom. Both parts are computed over the whole radius region.

3. Materials and methods

Noise-free synthetic data were generated by the finite element method [9,10] and analyzed for the simultaneous determination of sedimentation and diffusion coefficients. Radial concentration profiles were calculated for proteins or peptides of various molecular masses from 0.4 to 7.000 kDa. The concentration profiles were finished by a concentration (optical density) = 3. Therefore the later profiles reach not always the bottom radius. Different speeds between 10 000 and 60 000 rev./min were used as appropriate based on the expected sedimentation velocity of the substances. The curves between the meniscus radius $r_m = 6.3$ cm and the cell base $r_b = 7.2$ cm were presented by 1.801 data points and a radial step length of 0.0005 cm and a simulation time step $dt = 0.5$ s.

3.1. Program LAMM

A computer program, LAMM [8,16], was written in Delphi for the use in a windows personal computer. The program reads up to 300 XL-A data files, which are simultaneously fitted (global fit) and estimates the sedimentation and diffusion coefficients as well as the loading concentration, the baseline offset and the meniscus and bottom radii directly from the time-dependent records of radial concentration distributions. Further details of the program and the numerical methods used for estimation of the parameters are published in Demeler et al. [18]. The function (28) with the mentioned empirical improvements has also been added to our program. Sedimentation and diffusion coefficients together with the partial specific volume were used to calculate the molecular mass M by means of the Svedberg equation. Because function (28) is composed of two additional parts a control parameter is included in our program to prove the independence of them. Additionally, it is possible to present both curve parts on the monitor after finished iteration. The control parameter is based on determination of the gradient $dc/dr/c_0$ of both curve sections of the last data set at the radius position where they are parallel. In ideal case the gradient is 0, however, a small increase can be tolerated. The exact value also depends on the parameter ε, which determines the shape of both curve sections. A suitable test is the relation [Eq. (29)]. The observed small dependence on meniscus radius is described by use of a logarithmic normal distribution.

$$h = 1 + 2.2175(r_m - 6.3114) \quad (29)$$

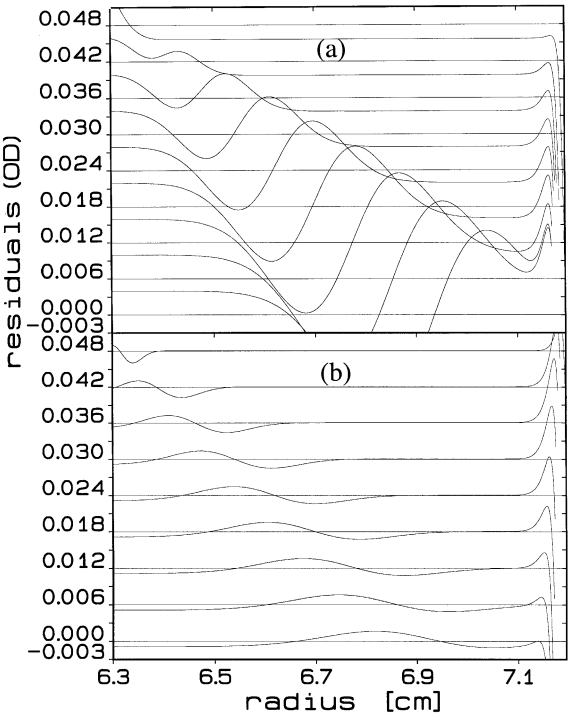

Fig. 1. Comparison of the residuals calculated with Eq. (3) (a) and Eq. (28) without empirical alterations (b). Claverie simulation for $s = 20$ S and $D = 2.6 \times 10^{-7}$ cm^2/s, $c_0 = 1$, rev./min = 13 000, $r_m = 6.3$ cm, $r_b = 7.2$ cm, time step 1000 s top to down. Only each third trace is shown. The following data were recovered: (a) $s = 20.05$ S, $D = 2.627 \times 10^{-7}$ cm^2/s, $c_0 = 0.994$, $r_m = 6.2999$ $r_b = 7.2001$, SSR = 1.09; (b) $s = 19.98$ S, $D = 2.638 \times 10^{-7}$ cm^2/s, $c_0 = 1.001$, $r_m = 6.3001$, $r_b = 7.2000$, SSR = 0.10.

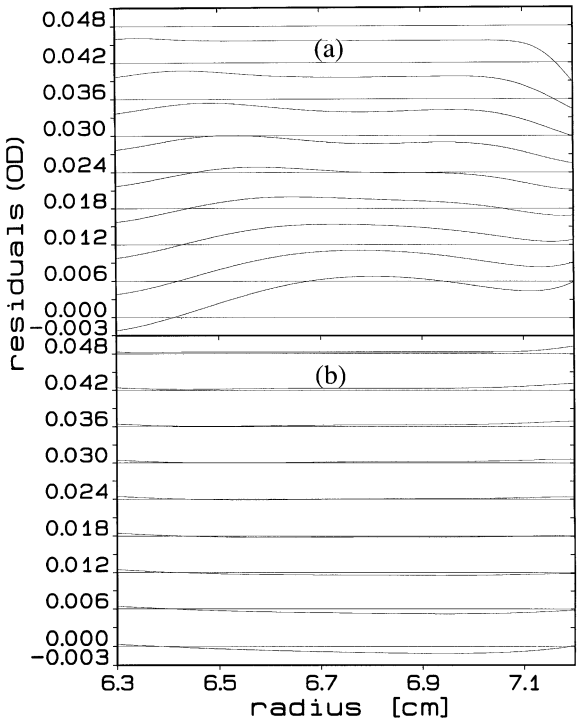

Fig. 2. Comparison of the residuals calculated with Eq. (5) (a) and Eq. (28) without empirical alterations (b). Claverie simulation for $s=0.23$ S and $D=28.5\times10^{-7}$ cm^2/s, $c_0=1$, 60 000 rev./min, $r_m=6.3$ cm, $r_b=7.2$ cm, time step 650 s top to down. Only each third trace is shown. The following data were recovered: (a) $s=0.233$ S, $D=28.51\times10^{-7}$ cm^2/s, $c_0=0.998$, $r_m=6.2994$, $r_b=7.2034$, SSR=0.309; (b) $s=0.230$ S, $D=28.54\times10^{-7}$ cm^2/s, $c_0=1.000$, $r_m=6.3000$, $r_b=7.1996$, SSR=0.072.

$$k=0.335+\frac{0.7826}{h}\exp\big(-\ln(h)\big(1.211\ln(h)-1\big)\big)$$

$$\text{gradient}<\frac{2.5k}{(1+35\varepsilon)}$$

The attainment of this condition for large values of ε (*small molecules*) is experimentally somewhat difficult, since in these cases the plateau is barely attained. By using a high rotor speed the ε values become smaller. A large column height is not favorable per se because it simultaneously enlarges ε. When the control parameter is too high >1 than some of the last data sets (in time) have to be omitted. But it is generally possible to obtain sufficient data files also for small molecules, which fulfill this criterion.

4. Results

Eq. (28) was tested extensively on 19 synthetic noise free data sets generated according to Claverie et al. [9] and Cox and Dale [10], which enclose the whole region of molecular mass of practical interest (0.4–7000 kDa). As shown by the residual plots (Figs. 1 and 2) of two selected examples with different sedimentation and diffusion coefficients the fit quality of Eq. (28) is much better than the former solution [Eq. (5)] particularly at higher sedimentation coefficients. Nevertheless,

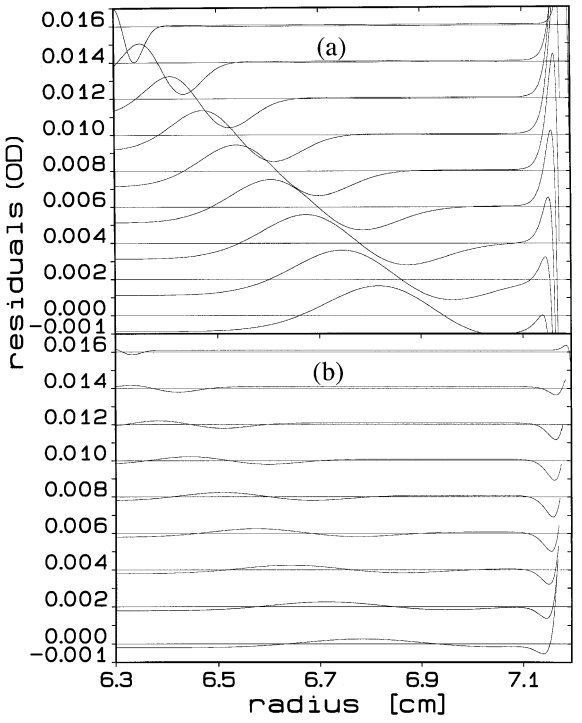

Fig. 3. Comparison of the residuals calculated with Eq. (28) without (a) and with empirical alteration (b). Claverie simulation for $s=20$ S and $D=2.6\times10^{-7}$ cm^2/s, $c_0=1$, 13 000 rev./min, $r_m=6.3$ cm, $r_b=7.2$ cm, time step 1000 s top to down. Only each third trace is shown. The following data were recovered: (a) $s=19.98$ S, $D=2.638\times10^{-7}$ cm^2/s, $c_0=1.001$, $r_m=6.3001$, $r_b=7.2000$, SSR=0.10; (b) $s=20.00$ S, $D=2.604\times10^{-7}$ cm^2/s, $c_0=1.000$, $r_m=6.3000$, $r_b=7.2000$, SSR=0.0018.

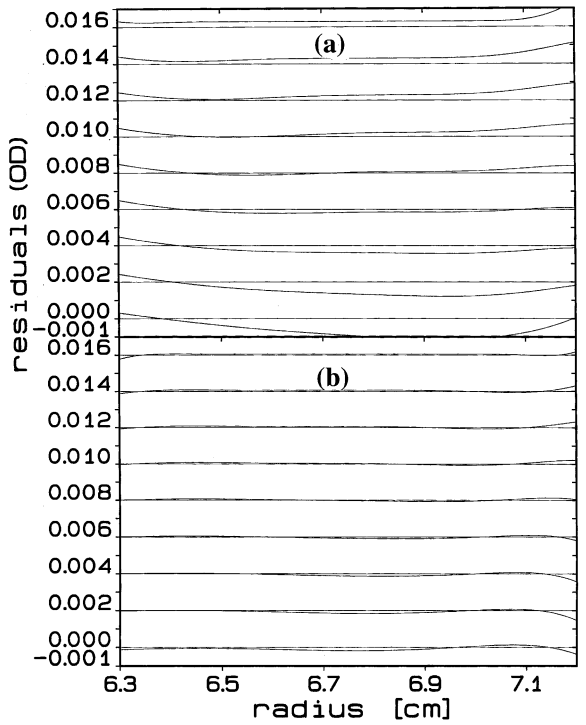

Fig. 4. Comparison of the residuals calculated using Eq. (28) without (a) and with empirical alteration (b). Claverie simulation for $s=0.23$ S and $D=28.5\times10^{-7}$ cm^2/s, $c_0=1$; 60 000 rev./min, $r_m=6.3$ cm, $r_b=7.2$ cm, time step 650 s top to down. Only each third trace is shown. The following data were recovered: (a) $s=0.230$ S, $D=28.54\times10^{-7}$ cm^2/s, $c_0=1.000$, $r_m=6.3000$, $r_b=7.1996$, SSR=0.072; (b) $s=0.229$ S, $D=28.33\times10^{-7}$ cm^2/s, $c_0=1.000$, $r_m=6.3002$, $r_b=7.2000$, SSR=0.0003.

even more accuracy is desirable. By trial and error it was found that slight empirical modifications of the variables z and ε_b in the bottom part of Eq. (28) can improve the accuracy considerably. The two quantities a and c are definable by ε-dependent functions described by asymmetric bell curves (logarithmic normal distribution). The parameters of the two functions (30,31) are estimated by fitting the values obtained for the 19 data sets.

$$z=2\frac{r}{r_b}\left(1+a\varepsilon(e^{\tau/2}-1)\right)-2 \qquad (30)$$

$$\varepsilon_b=\frac{2D}{r_b^2 s\,\omega^2}\left(1+c\varepsilon(e^{\tau/2}-1)\right)$$

$$a=\frac{9.107}{p}\exp\left(-\ln(p)\left(0.1783\ln(p)-1\right)\right)+2.4917 \qquad (31)$$

$$p=1+84.08(\varepsilon-0.01234)$$

$$c=\frac{0.2713}{h}\exp\left(-\ln(h)\left(0.02147\ln(h)-1\right)\right)-0.091$$

$$h=1+455.75(\varepsilon-0.0025395)$$

The improvements achieved by these empirical alterations are shown in the residual plots of Figs. 3 and 4. Furthermore, the square sum of residuals (SSR) was strongly diminished. Obviously this is of great advantage particularly when fitting data with high background noise because the shape of

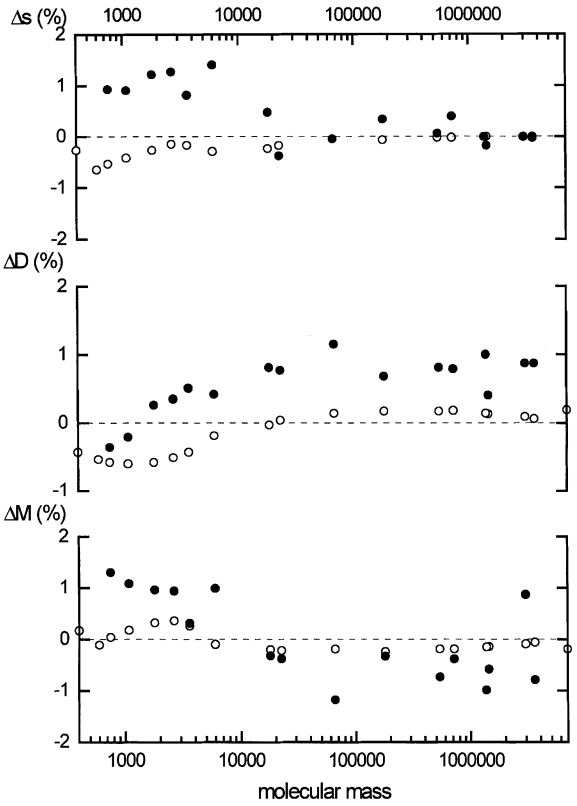

Fig. 5. Plots of the deviations of estimated sedimentation coefficients (above), diffusion coefficients (middle) and molecular masses (below) dependent on the size of macromolecules. The parameters were calculated from theoretical curves (Claverie simulations) using Eq. (28) including the empirical alterations (○) in comparison with Eq. (5) (●).

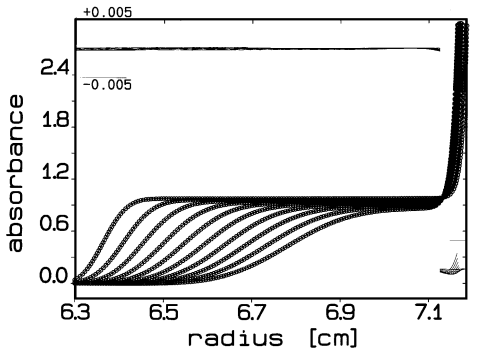

Fig. 6. Claverie simulation for $s=4.0$ S and 6.0×10^{-7} cm^2/s, $c_0=1$ and 40 000 rev./min, $r_m=6.3$ cm, $r_b=7.2$ cm, $\varepsilon=0.00432$. The following data were recovered: $s=3.999\pm1.19\times10^{-8}$ S, $D=(6.012\pm3.8\times10^{-5})10^{-7}$ cm^2/s, $c_0=1.0005$; $r_m=6.3000$ cm, $r_b=7.2000$ cm. Residuals are given at 64-fold amplification. From the 22 data sets generated in time intervals of 500 s and used for the fitting procedure only every third is shown.

the true concentration profiles is much better simulated.

In order to demonstrate the quality of the improved model function including the empirical alterations all 19 synthetic data sets generated for sedimentation coefficients between 0.14 and 90 S and diffusion coefficients between 32×10^{-7} cm^2/s and 1.2×10^{-7} cm^2/s were fitted. The deviations from the expected values including the molecular mass data (in percentage) are presented in Fig. 5. The deviations are smaller than 1% for all curves in the above-mentioned molecular mass region. Additionally to the sedimentation and diffusion coefficients in the global fitting procedure the loading concentration (c_0) as well as the radius position at the meniscus or cell base were estimated simultaneously. Only the base line was held constant. The estimated s and D values are in excellent agreement with the expected ones. Consequently, the molecular mass values were also obtained with high accuracy. In addition, the position of meniscus and bottom radii is estimated to a precision better than 0.0003 cm. In contrast with our former variant, the fit quality was considerably improved. The average square deviation SSR was diminished by 1–2 orders of magnitude. Fig. 6 demonstrates a typical whole boundary diagram of sedimentation traces for $s=4$ S, $D=6\times10^{-7}$ cm^2/s and the fitting results obtained with program LAMM. As can be seen from the residuals the fit at the meniscus boundary is excellent whereas the bottom boundary shows some small deviations.

5. Discussion

The new alterations in the model function representing an approximate solution of the Lamm equation clearly improved the precision of sedimentation and diffusion coefficients derived from fits of the radial concentration distribution. The deviations from the expected results are smaller than 1% for simulated curves and are valid for a great range of molecular masses from 0.4 to at least 7000 kDa. The presented approximate solution, an essential part of LAMM allows the estimation of s and D with an accuracy comparable to that achieved using numerical solutions, e.g the program SEDFIT of Schuck et al. [13,14] (RASMB release 8). The first three terms of function (28) are also a very excellent approximation for a solution of the Lamm equation when only considering the meniscus boundary condition (Faxén type) and has been incorporated into LAMM. The presented whole boundary solution [Eq. (28)] fits both the moving boundary and the accumulated solute near the cell base with high accuracy. Only the same fit quality in both curve sections is a guarantee for homogenous solutions. Solute inhomogeneities, e.g. by small amounts of aggregates can be recognized easily by more or less deviations in the curve fits. Therefore, the successful application of this procedure is suitable to declare the solute quality.

LAMM's improvements are based on the altered model function and that all whole boundary curves near the cell base can be cut individually or can finish at a common absorbance, respectively. These conditions can yield more information compared with the procedure of uniform fixed bottom radius as proposed in the program SEDFIT [13]. The program LAMM works with derivatives to the estimating parameters. The computation of the derivatives requires no additional calculations of error functions because the derivatives result in

simply exponential functions. This is in contrast to the numerical calculated difference quotients, which require two additional time consuming computations of the numerical Lamm solution for each parameter. Therefore the numerical programs available for the whole boundary [12,13] employ fitting methods without use of difference quotients. Therefore, even with bad starting values, they converge much better compared with the numerical approaches [12,13]. This is of advantage, contrary to the numerical approaches mentioned above, but the latter appear to yield more exact results. A further advantage of the program LAMM is that no starting values are necessary, they were generated automatically. Moreover, the data derived from the program LAMM can be used as *very good* starting values for using the program SEDFIT. LAMM provides this procedure as a special option and yields the edited data sets together with the estimated parameters in a format for direct loading by the program SEDFIT (list.ra9, ~temppars.ra9). The program SEDFIT in principle does not have the problem with dependent partial traces as valid for program LAMM. The numerical solution according to Claverie et al. [9] considers simultaneously both boundary conditions without any restrictions. For data sets with a low signal-to-noise ratio and a meniscus that is not free of solute, it is desirable to determine the loading concentration or extinction using the value obtained at 3000 rev./min or from the first (early) concentration profile and attain this value during the fitting procedure. The program LAMM offers an option for absorbency data for this.

Acknowledgments

The authors are grateful to Dr Howard Etlinger for careful reading this manuscript. The new version LAMM will be available at rasmb@alpha.bbri.org.

References

[1] S.E. Harding, A.J. Rowe, J.C. Horton (Eds.), Analytical Ultracentrifugation in Biochemistry and Polymer Science, Royal Soc, Cambridge, 1992.
[2] T.M. Schuster, T.M. Laue (Eds.), Modern Analytical Ultracentrifugation, Birkhäuser, Boston, 1994.
[3] O. Lamm, Die Differentialgleichung der Ultrazentrifugierung, Ark. Mat. Astr. Fys. 21B (1929) 1–6.
[4] H. Fujita, Mathematical Theory of Sedimentation Analysis, Academic Press, New York, 1962.
[5] L.A. Holladay, An Approximate Solution to the Lamm Equation, Biophys. Chem. 10 (1979) 187–190.
[6] J.S. Philo, Measuring sedimentation, diffusion, and molecular weights of small molecules by direct fitting of sedimentation velocity concentration profiles, in: T.M. Schuster, T.M. Laue (Eds.), Modern Analytical Ultracentrifugation, Birkhauser, 1994.
[7] J.S. Philo, An improved function for fitting sedimentation–velocity data for low-molecular-weight solutes, Biophys. J. 72 (1997) 435–444.
[8] J. Behlke, O. Ristau, Molecular-mass determination by sedimentation–velocity experiments and direct fitting of the concentration profiles, Biophys. J. 72 (1997) 428–434.
[9] J.M. Claverie, H. Dreux, R. Cohen, Sedimentation of generalized systems of interacting particles. I. Solution of systems of complete Lamm equations, Biopolymers 14 (1975) 1685–1700.
[10] D.J. Cox, R.S. Dale, Simulation of transport experiments for interacting systems, in: C. Frieden, L.W. Nichol (Eds.), Protein–Protein Interaction, Wiley, New York, 1981, pp. 173–201.
[11] B. Demeler, H. Saber, J.C. Hansen, Identification and interpretation of complexity in sedimentation velocity boundaries, Biophys J. 72 (1997) 397–407.
[12] B. Demeler, H. Saber, Determination of molecular parameters by fitting sedimentation data to finite-element solutions of the Lamm equation, Biophys. J. 74 (1998) 444–454.
[13] P. Schuck, C.E. MacPhee, G.J. Howlett, Biophys. J. 74 (1998) 466–474.
[14] P. Schuck, Sedimentation analysis of noninteracting and self-associating solutes using numerical-solutions to the Lamm equation, Biophys. J. 75 (1998) 1503–1512.
[15] P. Schuck, B. Demeler, Direct sedimentation analysis of interference optical data in ultracentrifugation, Biophys. J. 76 (1999) 2288–2296.
[16] J. Behlke, O. Ristau, An improved approximate solution of the Lamm equation for the simultaneous estimation of sedimentation and diffusion coefficients from sedimentation velocity experiments, Biophys. Chem. 70 (1998) 133–146.
[17] N.K. Hiester, T. Vermeulen, Saturation performance of ion-exchange and adsorbtion columns, Chem. Eng. Progr. 48 (1952) 505–516.
[18] B. Demeler, J. Behlke, O. Ristau, Molecular parameters from sedimentation velocity experiments: whole boundary fitting using approximate and numerical solutions of Lamm equation, Methods Enzymol. 321 (2000) 38–66.